Extended vector fitting for the assessment of subharmonics, harmonics, interharmonics, and supraharmonics in electrical systems

E.S. Bañuelos-Cabral, J.A. Gutiérrez-Robles, J.J. Nuño-Ayón,
J. Sotelo-Castañón, J.L. Naredo.

***Abstract* – The growth and integration of renewable energy and control systems in the utility grid represents a challenge for the electric power industry. Power quality monitoring plays a critical role in modern electrical systems for both standards compliance and system security reasons. This paper presents a novel technique for calculating subharmonics, harmonics, interharmonics, supraharmonics, and DC offset in electrical systems. This extended spectral fitting (ESF) approach is a combination of the numerical Laplace transform (NLT) and a modified vector fitting (VF) which we have denominated extended vector fitting (EVF). In this novel approach, it is assumed that frequencies of the harmonics and supraharmonics are known poles and that frequencies of the subharmonics and interharmonics are unknown poles in the frequency domain (FD), resulting in a rational approximation that considers known poles and unknown poles. The advantages of the proposed methodology are demonstrated (1) for synthetic test signals and (2) in an AC-DC-AC converter simulation. Results show that the ESF approach can fully decompose a signal into the aforementioned components with a high degree of accuracy.**

***Keywords*: Extended vector fitting, numerical Laplace transform, harmonics, interharmonics, supraharmonics.**

I. Introduction

POWER quality requirements in modern electrical systems are an important aspect to consider due to the integration of power electronics technologies associated with current renewable energy and control systems. Integrating these systems into the utility grid generates significant technical challenges to the power industry. For example, a large-scale integration of these technologies and their interaction with network elements can lead to power quality issues, such as subharmonic, harmonic, or interharmonic distortion in waveforms, which can lead to unstable operating conditions [1, 2]. Different problems have even been reported in medium- or low-voltage systems due to high frequency distortion or supraharmonics in the frequency range of 2-150 kHz [3, 4]. These components also negatively affect the electrical distribution system's power quality and reduce its efficiency [5].

Thus, proper identification of these components in electrical systems requires analytical tools which allow a precise estimation.

E.S. Bañuelos-Cabral, J.A. Gutiérrez-Robles, J.J. Nuño-Ayón and J. Sotelo-Castañón are with the University of Guadalajara, México (e-mail of corresponding author: jose.grobles@academicos.udg.mx).
J.L. Naredo is with Cinvestav, Guadalajara, México.
Paper submitted to the International Conference on Power Systems Transients (IPST2023) in Thessaloniki, Greece, June 12-15, 2023.

A comprehensive review of the available literature on harmonics estimation techniques was presented in [6] and includes discrete Fourier transform (DFT), wavelet transform (WT), Hilbert–Huang transform (HHT), Chirpz-transform (CZT), autoregressive moving average (ARMA), Prony's method, multiple signal classification (MUSIC), estimation of signal parameters via rotational invariance technique (ESPRIT), Kalman filtering (KF), artificial neural network (ANN), and phase locked loop (PLL), in which the advantages, disadvantages, main references, and potential applications for each technique is reviewed. More recently, the matrix pencil method [7] was proposed for calculating harmonics and interharmonics even in presence of noise. The sine cosine algorithm for accurate estimation of harmonics and interharmonics is presented in [8] and a hybrid method is presented and proposed for application online in [9].

This paper presents a novel technique for subharmonics, harmonics, interharmonics, supraharmonics, and DC offset calculation in electrical systems. The methodology consists of first obtaining the frequency domain (FD) image of a signal via the numerical Laplace transform (NLT) and then by using a rational approximation technique to calculate the DC offset, amplitude, damping, frequency, and phase of each aforementioned component. Vector fitting (VF) is the rational fitting technique used for this purpose. We called spectral fitting (SF) approach to the combination of the NLT and VF, and it had been implemented for the identification of electromechanical oscillation modes and mode shape [10]. Unlike that work, this one presents a novel modification of the VF algorithm that allows to identify the subharmonics, interharmonics, harmonics, supraharmonics, and DC offset at the same time. This extended VF (EVF) permits to carry out a rational approximation that considers known and unknown poles. We have now called extended spectral fitting (ESF) to the combination of the NLT and EVF.

This paper begins with a brief review of NLT theory. EVF and the ESF methodology are then explained in detail and latter demonstrated (1) for synthetic test signals and (2) in an AC-DC-AC converter simulation.

II. Extended spectral fitting (ESF) approach

A brief overview of the NLT theory is presented in this section, and the EVF method is shown on detail, which allows rational approximations with known and unknown poles. Finally, both techniques are interrelated in ESF.

A. Numerical Laplace transform (NLT)

For a signal $f(t)$, the unilateral Laplace Transform is defined as [11],

$$F(s) = \int_{o}^{\infty} f(t)e^{-st}dt, \tag{1}$$

where the complex frequency is given by $s = c + j\omega$, with ω being the angular frequency and c being a positive real constant. The NLT can be calculated by considering the independent variables discretized as [12, 13]

$$\begin{aligned} t_n &= n\Delta t, \qquad n = 0,1,\dots,N_s-1 \\ \omega_k &= k\Delta\omega, \qquad k = 0,1,\dots,N_s-1. \end{aligned} \tag{2}$$

Using (2) and the rectangular rule of integration in (1) gives,

$$F_k = \frac{T_{obs}}{N_s}\sum_{n=0}^{N_s-1}\left(f_n e^{-cTn/N_s}\right)e^{-j2\pi nk/N_s}, \tag{3}$$

where $F_k \equiv F(c + jk\Delta\omega)$ and $f_n \equiv f(n\Delta t)$. Regular sampling has been considered in (2) and (3), where $\Delta t = T_{obs}/N_s$ and $\Delta\omega = 2\pi/T_{obs}$ with T_{obs} being the observation time and N_s the number of samples. Note that (3) allows using the FFT algorithm.

On the other hand, if odd sampling is used for discretization of ω, (3) becomes,

$$F_{2k+1} = \frac{T_{obs}}{N_s}\sum_{n=0}^{N_s-1}\left(f_n e^{-(cT+j\pi)n/N_s}\right)e^{-j2\pi nk/N_s}, \tag{4}$$

where $F_{2k+1} \equiv F(c + j(2k+1)\Delta\omega)$ and $f_n \equiv f(n\Delta t)$, with $\Delta t = T_{obs}/N_s$ and $\Delta\omega = \pi/T_{obs}$. In this case, the discretized variables are [12, 13]

$$\begin{aligned} t_n &= n\Delta t, \qquad n = 0,1,\dots,N_s-1 \\ \omega_k &= (2k+1)\Delta\omega, \qquad k = 0,1,\dots,N_s-1. \end{aligned} \tag{5}$$

B. Extended vector fitting (EVF) method

Conventional process of VF [14] calculates a rational function-based model of a scalar function $F(s)$ on pole-residue form (6) by relocating a set of initial poles through an iterative procedure in a least-squares (LS) sense where coefficients d and h may be zero.

$$F(s) \cong \sum_{n=1}^{N}\frac{c_n}{s-p_n} + d + sh, \tag{6}$$

where c_n are the residues, p_n are the poles, d is a constant term and h is a proportional part for the rational approximation. Note that VF formulation assumes that all poles are unknown. Assuming now that some poles are known and others are unknown, we get,

$$F(s) \cong \sum_{n=1}^{N_1}\frac{c'_n}{s-p_{l_n}} + \sum_{n=1}^{N_2}\frac{c_n}{s-p_{v_n}} + d + sh, \tag{7}$$

where c'_n are the residues of the known poles p_{l_n} and c_n are the residues of the unknown poles p_{v_n}. Equation (7) indicates that it is possible to assume that some poles of the rational approximation may be known. In ESF is assumed that frequencies of the harmonics and supraharmonics are known poles in the FD and that frequencies of the subharmonics or interharmonics are unknown poles in the FD.

The VF algorithm works in two stages. First, it improves initial pole position iteratively. Second, it calculates the residues in a single step.

1) Unknown poles identification step

The goal in this step is to calculate the unknown poles for the rational approximation, which complete the set of poles for the fitting when added to the known poles. The initial pole set is defined as a_n and is improved through an iterative procedure. On each iteration, (8) can be solved with known poles p_{l_n} and a_n, where $\sigma(s)$ is an auxiliary weighting function (9) containing the same poles as in (8).

$$\sigma(s)F(s) \cong \sigma F_{fit}(s) = \sum_{n=1}^{N_1}\frac{c'_n}{s-p_{l_n}} + \sum_{n=1}^{N_2}\frac{c_n}{s-a_n} + d + sh. \tag{8}$$

$$\sigma(s) \cong \sigma_{fit}(s) = \sum_{n=1}^{N_1}\frac{\tilde{c}'_n}{s-p_{l_n}} + \sum_{n=1}^{N_2}\frac{\tilde{c}_n}{s-a_n} + 1, \tag{9}$$

with $\sigma F_{fit}(s)$ being the fitting of $\sigma(s)F(s)$and $\sigma_{fit}(s)$ being the fitting of $\sigma(s)$. Manipulating (8) results in,

$$F(s) \cong \frac{\sigma F_{fit}(s)}{\sigma(s)}. \tag{10}$$

Substituting (8) and (9) into (10) returns,

$$F(s) \cong h\frac{\left[\prod(s-z'_n)\Big/\prod(s-p_{l_n})\right]\cdot\left[\prod(s-z_n)\Big/\prod(s-a_n)\right]}{\left[\prod(s-\tilde{z}'_n)\Big/\prod(s-p_{l_n})\right]\cdot\left[\prod(s-\tilde{z}_n)\Big/\prod(s-a_n)\right]}, \tag{11a}$$

$$F(s) \cong h\frac{\prod(s-z'_n)\cdot\prod(s-z_n)}{\prod(s-\tilde{z}'_n)\cdot\prod(s-\tilde{z}_n)}. \tag{11b}$$

Equation (11b) clearly states that the zeros from $\sigma(s)$ approximate the poles from $F(s)$. Furthermore, multiplying (9) by $F(s)$ results in,

$$\sigma(s)F(s) \cong \left[\sum_{n=1}^{N_1}\frac{\tilde{c}'_n}{s-p_{l_n}} + \sum_{n=1}^{N_2}\frac{\tilde{c}_n}{s-a_n} + 1\right]F(s). \tag{12}$$

Equating equations (8) and (12) yields,

$$\begin{aligned} &\sum_{n=1}^{N_1}\frac{c'_n}{s-p_{l_n}} + \sum_{n=1}^{N_2}\frac{c_n}{s-a_n} + d + sh = \\ &\left[\sum_{n=1}^{N_1}\frac{\tilde{c}'_n}{s-p_{l_n}} + \sum_{n=1}^{N_2}\frac{\tilde{c}_n}{s-a_n} + 1\right]F(s). \end{aligned} \tag{13}$$

Algebraic manipulation in (13) returns,

$$\begin{aligned} &\sum_{n=1}^{N_1}\frac{c'_n}{s-p_{l_n}} + \sum_{n=1}^{N_2}\frac{c_n}{s-a_n} + d + sh - \\ &\sum_{n=1}^{N_1}\frac{\tilde{c}'_n F(s)}{s-p_{l_n}} - \sum_{n=1}^{N_2}\frac{\tilde{c}_n F(s)}{s-a_n} = F(s). \end{aligned} \tag{14}$$

Equation (14) can now be formulated as a LS problem, **Ax** = **b**. Frequently, the sample size of the frequency response k is greater than the number of coefficients to be calculated, so an overdetermined system is obtained:

$$\mathbf{A}_k = \left[\frac{1}{s_k - p_{l_1}} \cdots \frac{1}{s_k - p_{l_{N_1}}} \quad \frac{1}{s_k - a_1} \cdots \frac{1}{s_k - a_{N_2}} \quad 1 \quad s_k \quad -\frac{F(s_k)}{s_k - p_{l_1}} \cdots -\frac{F(s_k)}{s_k - p_{l_{N_1}}} \quad -\frac{F(s_k)}{s_k - a_1} \cdots -\frac{F(s_k)}{s_k - a_{N_2}}\right]. \tag{15a}$$

$$\mathbf{x} = \left[c'_1 \cdots c'_{N_1} \quad c_1 \cdots c_{N_2} \quad d \quad h \quad \tilde{c}'_1 \cdots \tilde{c}'_{N_1} \quad \tilde{c}_1 \cdots \tilde{c}_{N_2}\right]^T. \tag{15b}$$

$$\mathbf{b} = [F(s_1) \quad \cdots \quad F(s_k)]^T. \tag{15c}$$

The LS solution of (15) delivers the residues of $\sigma_{fit}(s)$; the zeros of this function are the poles a_n for the next iteration, which correspond to the eigenvalues of [14],

$$\mathbf{H} = \mathbf{G} - \mathbf{k}\tilde{\boldsymbol{c}}^{\boldsymbol{T}}, \tag{16}$$

where $\mathbf{G}$ is a diagonal matrix with the poles and $\mathbf{k}$ is a unit column vector.

2) Residue identification step

Once the unknown poles p_{v_n} for the rational approximation in (7) have been calculated, the residues can be found by solving (7) as a LS problem.

C. Extended spectral fitting (ESF) approach

Let's begin by considering a power electrical signal defined by,

$$f(t) \cong \left[\psi + \sum_{n=1}^{N_1} A_{H_n} \cos\left(n\omega_0 t + \theta_{H_n}\right)\right] + \left[\sum_{n=1}^{N_c} A_{I_n} e^{\alpha_{I_n} t} \cos\left(\omega_n t + \theta_{I_n}\right) + \sum_{n=1}^{N_r} A_{R_n} e^{\alpha_{R_n} t}\right]. \tag{17}$$

The first square bracket of (17) is the compact representation of the Fourier series for N_1 harmonics or supraharmonics with fundamental frequency of $\omega_0 = 2\pi f_o$ and where A_{H_n} is the amplitude and θ_{H_n} is the phase for the *n*th component; and where ψ represents the DC offset.

Otherwise, the second square bracket of (17) considers N_c subharmonics or interharmonics with a frequency of $\omega_n = 2\pi f_n$ and a damping factor of α_{I_n}, where A_{I_n} is the amplitude and θ_{I_n} is the phase for the *n*th component; it also considers N_r exponential functions of amplitude A_{R_n} with a damping factor of α_{R_n}. It is assumed that $N_2 = N_c + N_r$.

The Laplace transform $F(s)$ of (17) can be expressed as [10, 11],

$$F(s) \cong \left[\frac{\psi}{s} + \sum_{n=1}^{N_1}\left(\frac{0.5A_{H_n}e^{j\theta_{H_n}}}{s - jn\omega_0} + \frac{0.5A_{H_n}e^{-j\theta_{H_n}}}{s + jn\omega_0}\right)\right] + \left[\sum_{n=1}^{N_c}\left(\frac{0.5A_{I_n}e^{j\theta_{I_n}}}{s - \alpha_{I_n} - j\omega_n} + \frac{0.5A_{I_n}e^{-j\theta_{I_n}}}{s - \alpha_{I_n} + j\omega_n}\right) + \sum_{n=1}^{N_r}\frac{A_{R_n}}{s - \alpha_{R_n}}\right]. \tag{18}$$

The use of (18) is inconvenient because in the LS implementation of VF, and even in other rational approximation methods [15], a pole in the origin is not considered. However, this drawback can be overcome; an artificially damped function in the time domain (TD) (20) and a rational frequency-shifting response in the FD (21) are obtained by applying the frequency-shifting property (19) [11] to (17) and (18).

$$f(t)e^{\lambda t} = F(s - \lambda). \tag{19}$$

$$f(t) \cong \left(\left[\psi + \sum_{n=1}^{N_1} A_{H_n}\cos\left(n\omega_0 t + \theta_{H_n}\right)\right] + \left[\sum_{n=1}^{N_c} A_{I_n} e^{\alpha_{I_n} t}\cos\left(\omega_n t + \theta_{I_n}\right) + \sum_{n=1}^{N_r} A_{R_n} e^{\alpha_{R_n} t}\right]\right) e^{\lambda t}. \tag{20}$$

$$F(s - \lambda) \cong \left[\frac{\psi}{s - \lambda} + \sum_{n=1}^{N_1}\left(\frac{0.5A_{H_n}e^{j\theta_{H_n}}}{s - \lambda - jn\omega_0} + \frac{0.5A_{H_n}e^{-j\theta_{H_n}}}{s - \lambda + jn\omega_0}\right)\right] + \left[\sum_{n=1}^{N_c}\left(\frac{0.5A_{I_n}e^{j\theta_{I_n}}}{s - \lambda - \alpha_{I_n} - j\omega_n} + \frac{0.5A_{I_n}e^{-j\theta_{I_n}}}{s - \lambda - \alpha_{I_n} + j\omega_n}\right) + \sum_{n=1}^{N_r}\frac{A_{R_n}}{s - \lambda - \alpha_{R_n}}\right]. \tag{21}$$

Through the artificial damping function $e^{\lambda t}$, it is possible to dissipate the DC offset, ψ, which becomes a residue of a simple pole with known frequency, λ. The parameter identification of (20) can be done in the FD by using the EVF algorithm presented in the previous section once the image of $f(t)$ is numerically calculated through (3) or (4).

The first square bracket in (21) represents a function with known poles; a simple pole for the direct component ψ and N_1 conjugate complex poles with known frequencies for the harmonics or supraharmonics. And, the second square bracket of (21) represents a function with unknown conjugate complex poles for the subharmonics or interharmonics with or without damping and, possibly, simple real poles representing decreasing exponential functions in TD. The parameter identification of (17) can be now calculated. EVF delivers a function in pole-residue form with real poles and residues and with conjugate complex poles and residues as,

$$F(s) \cong \left[\frac{r_H}{s - p_{H_n}} + \sum_{n=1}^{N_1}\left(\frac{\gamma_{H_n} + j\eta_{H_n}}{s - \delta_{H_n} - j\beta_{H_n}} + \frac{\gamma_{H_n} - j\eta_{H_n}}{s - \delta_{H_n} + j\beta_{H_n}}\right)\right] + \left[\sum_{n=1}^{N_c}\left(\frac{\gamma_{I_n} + j\eta_{I_n}}{s - \delta_{I_n} - j\beta_{I_n}} + \frac{\gamma_{I_n} - j\eta_{I_n}}{s - \delta_{I_n} + j\beta_{I_n}}\right) + \sum_{n=1}^{N_r}\frac{r_{I_n}}{s - p_{I_n}}\right]. \tag{22}$$

Finally, the DC offset, amplitude, and phase of each harmonic or supraharmonic using the first square bracket in (21) and (22) are

$$\lambda = p_{H_n} = \delta_{H_n};\quad \psi \cong r_H;\quad n\omega_0 = n2\pi f_0 = \beta_{H_n};\quad \frac{A_{H_n}}{2}e^{j\theta_{H_n}} \cong \gamma_{H_n} + j\eta_{H_n}. \tag{23}$$

For subharmonics or interharmonics with or without damping and damped exponential functions by using the second square bracket in (21) and (22), they are

$$\omega_n = 2\pi f_n \cong \beta_{I_n};\quad \frac{A_{I_n}}{2}e^{j\theta_{I_n}} \cong \gamma_{I_n} + j\eta_{I_n};\quad \alpha_{I_n} \cong \delta_{I_n} - \lambda;\quad A_{R_n} \cong r_{I_n};\quad \alpha_{R_n} \cong p_n - \lambda. \tag{24}$$

III. Test Cases

A. Synthetic test signals

1) Full-wave rectified sinusoidal signal

In this example, the NLT accuracy is evaluated using a synthetic signal and its analytical Laplace transform; the harmonics are then calculated using the ESF methodology and compared to those calculated analytically. The synthetic test signal is a full-wave rectified sinusoidal signal,

$$f(t) = |\sin(\omega_0 t)|, \tag{25}$$

where $\omega_0 = 2\pi f_0$ rad/s, $f_0 = 50$ Hz, $T_0 = 1/f_0 = 0.02$ s, and considering the absolute value, the new period is $T = 1/(2f_0) = 0.01$ s. The analytic Laplace transform of (25) is,

$$\mathcal{L}[f(t)] = \frac{1}{1-e^{-Ts}}\left[\frac{\omega_0 - \omega_0 e^{-(s+j\omega_0)T}}{s^2+{\omega_0}^2}\right]. \tag{26}$$

On the other hand, coefficients a_0, a_n and b_n for the trigonometric Fourier series of (25) are

$$a_0 = \frac{1}{T\omega_0}[-\cos(\omega_0 T)+1] \approx 0.6366, \tag{27}$$

$$a_n = \frac{2}{T}\left[\frac{\cos(T\omega_0)\cos(2Tn\omega_0)}{\omega_0(4n^2-1)} + \frac{2n\sin(2Tn\omega_0)\sin(T\omega_0)-1}{\omega_0(4n^2-1)}\right],\ \omega_0 \neq 0, \tag{28}$$

$$b_n = \frac{1}{T}\left[\frac{\sin(T\omega_0(2n-1))}{\omega_0(2n-1)} - \frac{\sin(T\omega_0(2n+1))}{\omega_0(2n+1)}\right],\ \omega_0 \neq 0, \tag{29}$$

and the coefficients c_0, c_n and θ_n for the compact Fourier series (31) of (25) are

$$c_0 = a_0;\ c_n = \sqrt{(a_n)^2+(b_n)^2};\ \theta_n = \tan^{-1}\left[\frac{-b_n}{a_n}\right] \tag{30}$$

$$f(t) = c_0 + \sum_{n=1}^{N} c_n \cos(2n\omega_0 t + \theta_n) \tag{31}$$

Fig. 1a shows the full-wave rectified sinusoidal signal with a $T_{obs} = 0.06$ s and with $\Delta t = 100\ \mu$s. The NLT of this data set using odd sampling (4) is presented in Fig. 1b together with the analytic Laplace transform and its respective deviation. Note that these parameters give a maximum frequency of 100 kHz in NLT implementation. This result shows that the NLT approximation of the analytical Laplace transform is very accurate.

The rational approximation of the NLT through EVF and its fitting deviation is shown in Fig. 1c for up to 25 harmonics; therefore, $N_1 = 50$ poles with a cutoff frequency of 1250 Hz. In this example only harmonics are calculated, so only the first square bracket in (22) is considered. Once the rational approximation (22) is complete, DC offset and harmonics are calculated using (23).

Approximation of the synthetic signal by means of the compact Fourier series and the ESF method and its absolute error is presented in Figs. 1a and 2a, respectively. Finally, both amplitude spectrums are presented in Figs. 2b and 2c. The DC offset, amplitudes, and phases calculated using the compact Fourier series and the ESF are shown in Table I for the first 5 harmonics. The results show high accuracy in harmonics calculation using the proposed method.

TABLE I
DC OFFSET, AMPLITUDES AND PHASES OF THE FIRST 5 HARMONICS CALCULATED BY USING THE COMPACT FOURIER SERIES AND THE ESF APPROACH FOR $N_1 = 50$.

	Compact Fourier series		ESF approach	
n	c_n	θ_n [°]	c_n	θ_n [°]
0	0.6366	-	0.6366	-
1	0.4244	180	0.4243	179.99
2	0.0849	180	0.0848	-179.99
3	0.0364	180	0.0363	179.99
4	0.0202	180	0.0201	-179.99
5	0.0129	180	0.0128	179.99

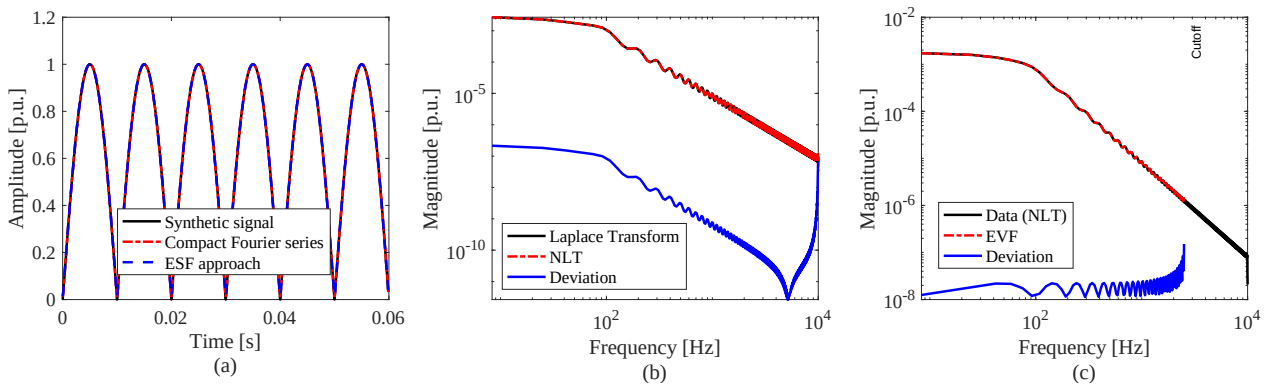

Fig. 1. (a) Full-wave rectified sinusoidal signal and its approximations, (b) analytic Laplace transform, NLT and its deviation, (c) NLT and fitting deviation.

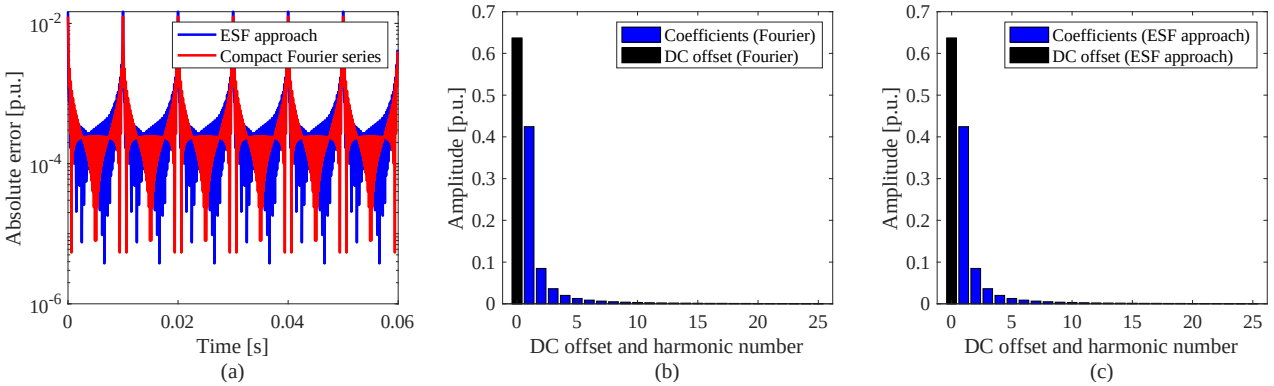

(a) (b) (c)

Fig. 2. (a) Absolute approximation error using the ESF and the compact Fourier series. Amplitude spectrum of the synthetic signal calculated by using (b) the compact Fourier series and, (c) the ESF approach.

2) Full-wave rectified sinusoidal signal plus subharmonics, interharmonics and a DC offset.

The proposed methodology is then evaluated using the full-wave rectified sinusoidal signal (25) to which two subharmonics, four interharmonics, an exponential function, and a DC offset are added,

$$\begin{aligned} f(t) = {} & |\sin(\omega_0 t)| + \\ & 0.5e^{-50t}\cos(2\pi 75t + 60°) + \\ & 0.8e^{-75t}\cos(2\pi 90t - 45°) + \\ & 0.2e^{-12t}\cos(2\pi 125t + 90°) + \\ & 0.2e^{-12t}\cos(2\pi 225t - 60°) + \\ & 0.7e^{-10t}\cos(2\pi 5025t + 0°) + \\ & 0.6e^{-45t}\cos(2\pi 7010t - 70°) + \\ & 0.3e^{-68t} + 1. \end{aligned} \tag{32}$$

The behavior of this synthetic test signal (32) is shown in Fig. 3a with a $T_{obs} = 0.06$ s and with $\Delta t = 100\,\mu s$. The NLT of the test signal is presented in Fig. 3b together with the fitting deviation using the EVF up to 100 harmonics, which is in the supraharmonic range. Therefore, $N_1 = 200$ poles in (22), resulting in a 10 kHz cutoff frequency. And for N_2, 20 poles are used. These 20 poles freely fitted in frequency, amplitude, damping, and phase. Once the approximation (22) is complete, the DC offset, amplitude, and phase of each harmonic or supraharmonic are calculated through (23); and through (24) for the subharmonics or interharmonics.

The ESF's synthetic signal approximation is presented separately in Fig. 3c, first for the sinusoidal rectified signal and the DC offset and then for the subharmonics and interharmonics; their absolute errors are presented in Fig. 4a. The complete synthetic signal approximation is presented in Fig. 3a and its absolute error in 4b. The amplitude spectrum is presented in Fig. 4c and the DC offset, amplitudes, and phases of the harmonics calculated by using the compact Fourier series and ESF are shown in Table 2 for the first 5 harmonics.

The parameters calculated by the ESF approach for $N_2 = 20$ are presented in Table 3. With these 20 poles, EVF converges to 2 real poles and 18 complex poles, returning 2 exponential functions and 9 sinusoidal functions in TD.

To discard those components spurious to the approximation, a relative dominant pole measurement (RDPM) $|c_n|/|p_n|$ is used [10]. This concept weights the position of the pole with respect to the residue size in the corresponding $F(s)$. Note that components 7, 8, 9, and 11 in Table 3 can be discarded by using this concept. By comparing (23) with the data in Table 3, the overall results show that the approximation is virtually the same.

TABLE II
DC OFFSET, AMPLITUDES, AND PHASES OF THE FIRST 5 HARMONICS CALCULATED BY USING THE COMPACT FOURIER SERIES AND THE ESF APPROACH FOR $N_1 = 200$.

	Compact Fourier series		ESF approach	
n	c_n	θ_n [°]	c_n	θ_n [°]
0	1.6366	-	1.6367	-
1	0.4244	180	0.4271	-179.96
2	0.0849	180	0.0849	179.99
3	0.0364	180	0.0364	179.99
4	0.0202	180	0.0202	179.99
5	0.0129	180	0.0129	179.99

TABLE III
AMPLITUDE, DAMPING, FREQUENCY, AND PHASE OF EACH COMPONENT CALCULATED BY THE ESF APPROACH FOR $N_2 = 20$.

	ESF approach				
n	A_{I_n}	α_{I_n}	f_n [Hz]	θ_{I_n} [°]	|RDPM|
1	0.5009	49.71	75.04	59.05	0.75
2	0.7938	75.35	90.19	-45.04	1.00
3	0.1999	11.95	124.99	90.10	0.18
4	0.2000	12.00	225.00	-60.00	0.10
5	0.6942	10.00	5025.00	-0.00	0.01
6	0.5904	44.99	7010.00	-70.00	0.01
7	4.8e-5	181.27	10082.50	-126.40	5e-7
8	3.0e-4	2.4e3	10416.01	-142.51	3e-6
9	0.0013	1.2e4	12853.98	-167.81	1e-5
10	0.3001	68.11	-	-	1.00
11	0.0004	1.3e5	-	-	0.00

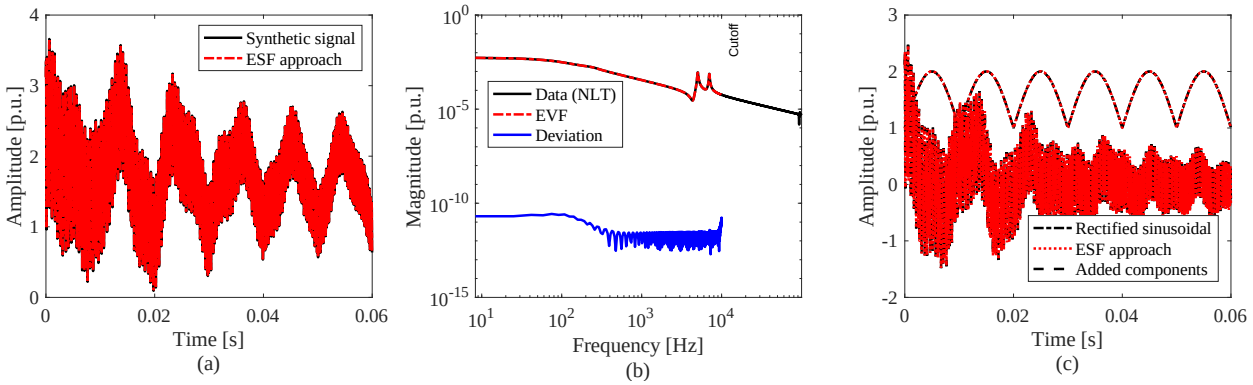

Fig. 3. (a) Synthetic test signal and its approximation, (b) NLT and fitting deviation, (c) rectified sinusoidal signal, added components and their approximations.

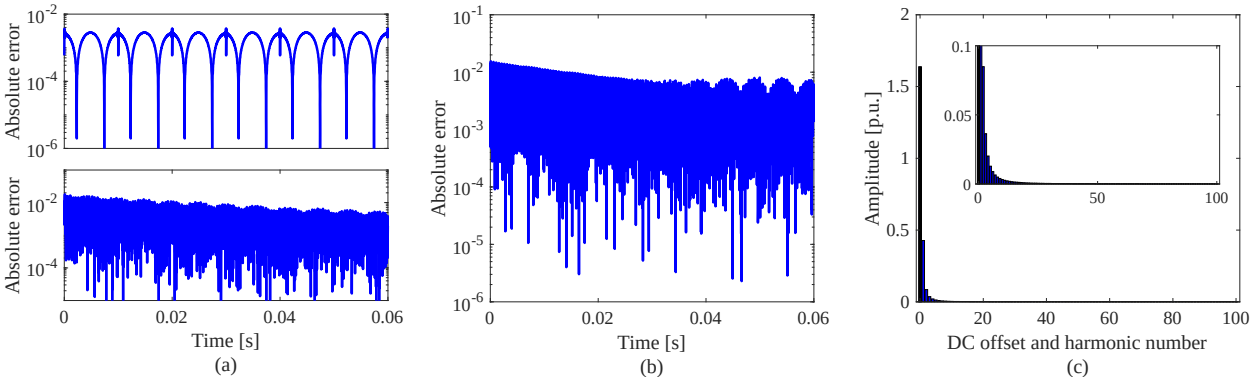

Fig. 4. (a) Absolute approximation error for the sinusoidal rectified signal and the DC offset and for added components, (b) absolute error for the complete approximation, (c) amplitude spectrum.

B. AC-DC-AC Converter

In this example, an AC-DC-AC converter model of Simulink is used to demonstrate the scope of the proposed methodology [16]. The test system, consisting of a 25 kV, 60 Hz voltage source which feeds a 50 kW, 50 Hz load through an AC-DC-AC converter, is shown in Fig. 5. The converter first uses a six-pulse diode bridge and then an IGBT two-level inverter to generate 50 Hz of voltage with the pulse width modulation (PWM) at a 2 kHz carrier frequency.

Note that the system is composed of three nodes: grid node, inverter node, and load node. The current at the grid node and its ESF approximation is presented in Fig. 6a for 100 harmonics, which uses $N_1 = 200$ and $N_2 = 30$ poles. The NLT of the signal is presented in Fig. 6b, which also shows the fitting deviation using the EVF up to 100 harmonics, 5 kHz.

From this point on, the subharmonics and interharmonics calculation are grouped as transient state; and the DC offset, the fundamental component, and harmonics as steady state. These results are shown in Fig. 6c with their respective scales.

Similarly, the results for the voltage in the inverter node are shown from Fig. 7a to Fig. 7c with $N_1 = 2$ and $N_2 = 1$ poles, so the cutoff frequency is 50 Hz.

Moreover, the results for the voltage in the inverter node with $N_1 = 2000$ and $N_2 = 20$ poles are shown from Fig. 8a to Fig. 8c; which are 1000 harmonics. Additionally, the absolute error for the approximation is presented in Fig. 9a and amplitude spectrum and phase spectrum in Figs. 9b and 9c, respectively. It can be highlighted how harmonics occur in multiples of the inverter switching frequency.

These results validate a good performance of the ESF approach for a wide frequency range.

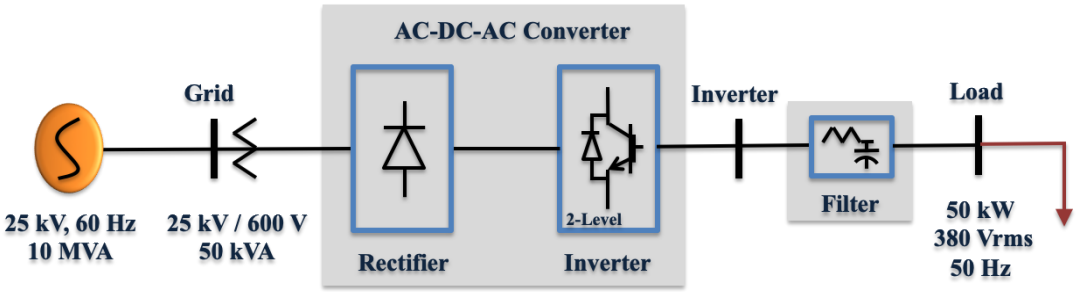

Fig. 5. AC-DC-AC Converter test system.

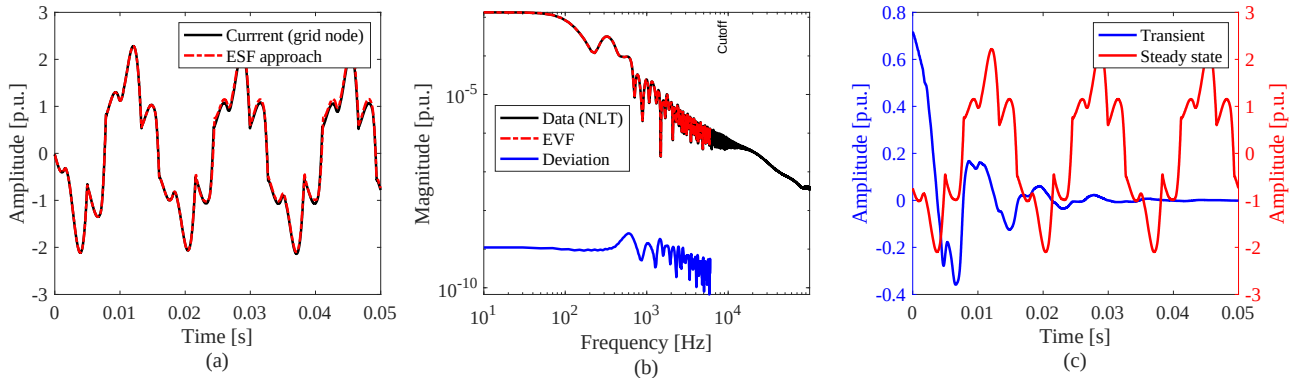

Fig. 6. (a) Current at the grid node and its approximation, (b) NLT and fitting deviation, (c) transient and steady state responses calculated by ESF.

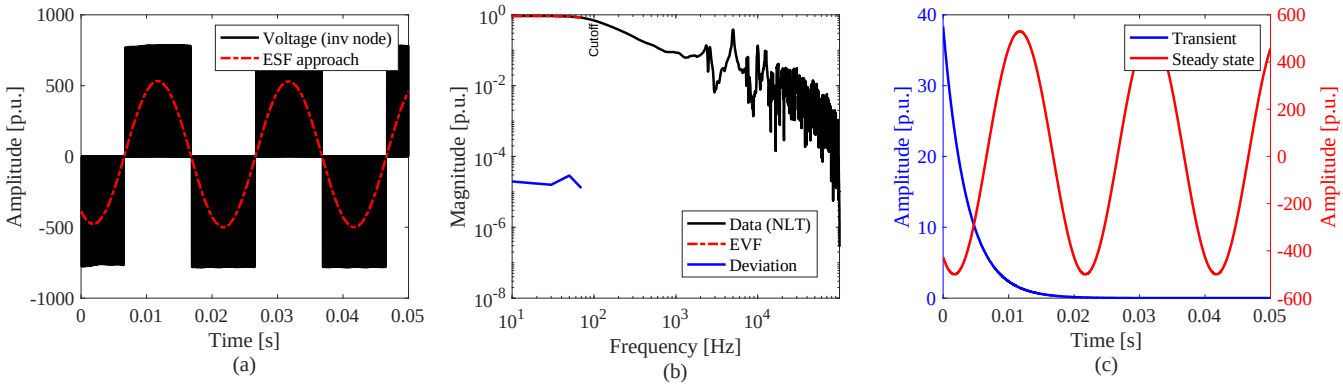

Fig. 7. (a) Voltage at the inverter node and its approximation, (b) NLT and fitting deviation, (c) transient and steady state responses calculated by ESF.

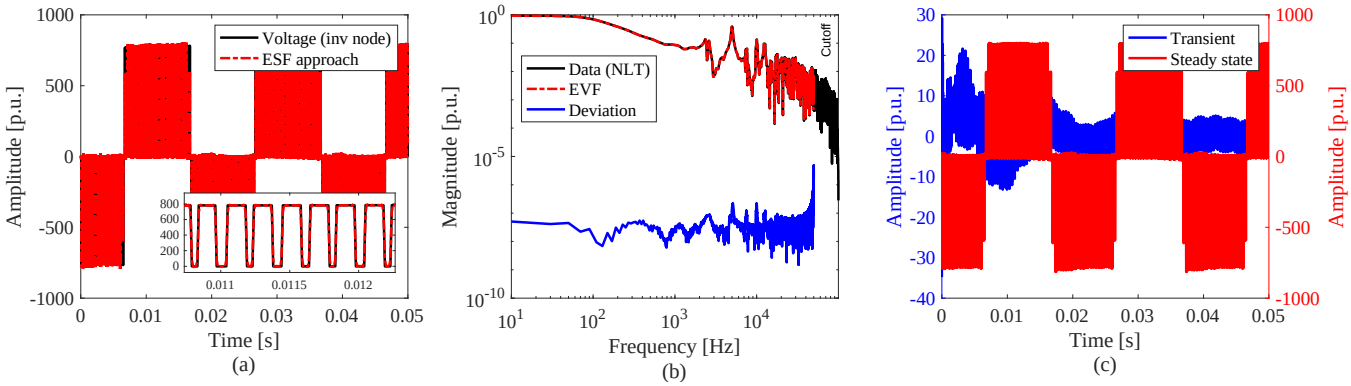

Fig. 8. (a) Voltage at the inverter node and its approximation, (b) NLT and fitting deviation, (c) transient and steady state responses calculated by ESF.

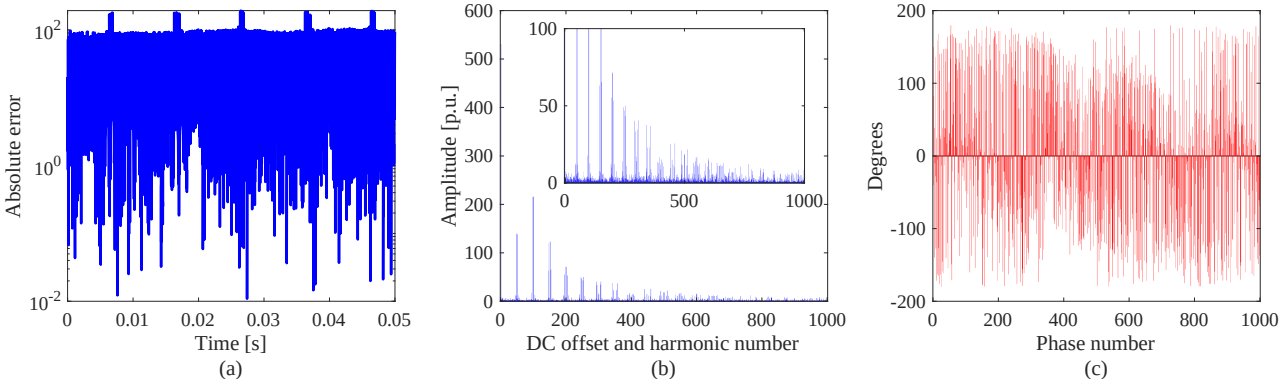

Fig. 9. (a) Absolute error for the voltage approximation at the inverter node, (b) amplitude spectrum for 1000 harmonics, (c) phase spectrum.

IV. Conclusions

The ESF approach was presented for the calculation of subharmonics, harmonics, interharmonics, supraharmonics, and DC offset in electrical systems. This methodology is a combination of the NLT and a novel modification of the VF, which the authors have denominated extended vector fitting (EVF). The main findings are as follows:

1) The EVF method assumes that some rational approximation poles are known, and others are unknown. This work presents one implementation of this feature; however, it could be used in other applications.
2) The ESF methodology is able to simultaneously calculate the amplitude and phase of each harmonic or supraharmonic; the amplitude, damping, frequency, and phase of each subharmonic or interharmonic; and the DC offset contained in a signal.
3) Parameter identification is calculated with high accuracy due to the error level achieved by both the NLT and the EVF.
4) The methodology can be used to obtain the phase of the fundamental component regardless of whether it has content of harmonics and interharmonics.
5) The results of the examples validate a good performance of the ESF approach for a wide frequency range.
6) Components spurious to rational approximation can be discarded by the RDPM.

V. References

[1] X. Liang, "Emerging power quality challenges due to integration of renewable energy sources," *IEEE Transactions on Industry Applications*. 53 (2017) 855–866. https://doi.org/10.1109/TIA.2016.2626253

[2] A.Q. Al-Shetwi, M.A. Hannan, K.P. Jern, M. Mansur, T.M.I. Mahlia, "Grid-connected renewable energy sources: Review of the recent integration requirements and control methods," *Journal of Cleaner Production*. 253 (2020) 119831. https://doi.org/10.1016/j.jclepro.2019.119831

[3] Á. Espín-Delgado, S. Rönnberg, T. Busatto, V. Ravindran, M. Bollen, "Summation law for supraharmonic currents (2–150 kHz) in low-voltage installations," *Electric Power Systems Research*. 184 (2020) 106325. https://doi.org/10.1016/j.epsr.2020.106325

[4] Á. Espín-Delgado, S. Rönnberg, S.S. Letha, M. Bollen, "Diagnosis of supraharmonics-related problems based on the effects on electrical equipment," *Electric Power Systems Research*. 195 (2021) 107179. https://doi.org/10.1016/j.epsr.2021.107179

[5] S.T.Y. Alfalahi et al., "Supraharmonics in power grid: Identification, standards, and measurement techniques," *IEEE Access*. 9 (2021) 103677 - 103690. https://doi.org/10.1109/ACCESS.2021.3099013

[6] S.K. Jain, S.N. Singh, "Harmonics estimation in emerging power system: Key issues and challenges," *Electric Power Systems Research*. 81 (2011) 1754 - 1766. https://doi.org/10.1016/j.epsr.2011.05.004

[7] K. Sheshyekani et al., "A general noise-resilient technique based on the matrix pencil method for the assessment of harmonics and interharmonics in power systems," *IEEE Transactions on Power Delivery*. 5 (2016) 2179 - 2188. https://doi.org/10.1109/TPWRD.2016.2625329

[8] C. Altintasi, "Sine cosine algorithm approaches for directly estimation of power system harmonics & interharmonics parameters," *IEEE Access*. 9 (2021) 73169 - 73181. https://doi.org/10.1109/ACCESS.2021.3081037

[9] R.J. Betancour et al., "A spatio-temporal processing Padé approach for visualizing harmonic distortion propagation on electrical networks," *Electric Power Systems Research*. 203 (2021) 73169 - 73181. https://doi.org/10.1016/j.epsr.2021.107643

[10] E.S. Bañuelos-Cabral et al., "Spectral fitting approach to estimate electromechanical oscillation modes and mode shapes by using vector fitting," *Electric Power Systems Research*. 176 (2019) 105958. https://doi.org/10.1016/j.epsr.2019.105958

[11] B.P. Lathi, *Principles of linear systems and signals*, second ed., Oxford university press, United Kingdom, 2009.

[12] P. Moreno, *Análisis de transitorios con la transformada numérica de Laplace*, second ed., Editorial Académica Española, España, 2012.

[13] P. Moreno, A. Ramirez, "Implementation of the numerical Laplace transform: a review," *IEEE Trans. Power Deliv*. 23 (May (4)) (2008) 2599–2609. https://doi.org/10.1109/TPWRD.2008.923404

[14] B. Gustavsen, A. Semlyen, "Rational approximation of frequency domain responses by vector fitting," *IEEE Transactions on Power Delivery*. 3 (1999) 1052 - 1061. https://doi.org/10.1109/61.772353

[15] E.S. Bañuelos-Cabral et al., "Enhancing the accuracy of rational function-based models using optimization," *Electric Power Systems Research*. 125 (2015) 83 - 90. https://doi.org/10.1016/j.epsr.2015.04.001

[16] Documentation, Simulation and Model-Based Design. MathWorks (2021). https://www.mathworks.com/products/simulink.html